Lab on a Chip

Devices and applications at the micro- and nanoscale

Accepted Manuscript

This article can be cited before page numbers have been issued, to do this please use: M. Janik, S. V. H. Hamidi, M. Koba, J. Perreault, R. Walsh, W. Bock and M. Smietana, *Lab Chip*, 2020, DOI: 10.1039/D0LC01069C.

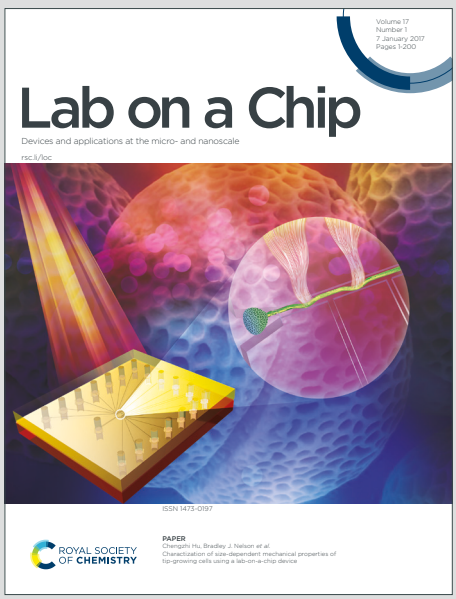

View Article Online
DOI: 10.1039/D0LC01069C

ARTICLE

Real-time isothermal DNA amplification monitoring in picoliter volumes using optical fiber sensor

Received 00th January 20xx,
Accepted 00th January 20xx

DOI: 10.1039/x0xx00000x

Monika Janik[1,2,*,‡], Seyed Vahid Hamidi[3,‡], Marcin Koba[1,4], Jonathan Perreault[3], Ryan Walsh[3], Wojtek J. Bock[5], Mateusz Śmietana[1]

Rolling circle amplification (RCA) of DNA can be considered as a great alternative to the gold standard polymerase chain reaction (PCR), especially during this pandemic period, where rapid, sensitive, and reliable test results for hundreds of thousands of samples are required daily. This work presents the first research to date on direct, real-time and label-free isothermal DNA amplification monitoring using microcavity in-line Mach Zehnder interferometer (µIMZI) fabricated in an optical fiber. The solution based on µIMZI offers a great advantage over many other sensing concepts – makes possible optical analysis in just picoliter sample volumes. The selectivity of the biosensor is determined by DNA primers immobilized on the microcavity's surface that act as selective biorecognition elements and triggers initiating the DNA amplification process. In this study, we verified the sensing concept using circular DNA designed to target the H5N1 influenza virus. The developed biosensor exhibits an ultrahigh refractive index sensitivity reaching 14,000 nm per refractive index unit and a linear detection range between 9.4 aM and 94 pM of the target DNA sequence. Within a 30 min period, the amplification of as little as 9.4 aM DNA can be effectively detected, with a calculated limit of detection as low as 0.2 aM DNA, suggesting this methodology holds great promise in practical disease diagnosis applications in the future.

Introduction

It has been more than thirty years since DNA amplification technologies were introduced and revolutionized molecular diagnostics.[1] Lately, interest in selective DNA amplification methods for diagnostics has become central to addressing the threat of the SARS-CoV-2 pandemic. Pandemic requires rapid, sensitive, and reliable test results for hundreds of thousands of samples daily. Invariably, the most frequently used techniques for detection rely on the polymerase chain reaction (PCR). PCR methods are based on the use of a thermostable enzyme (DNA polymerase) and thermocycler devices that can rapidly synthesize millions to billions of copies of a specific target DNA region. However, much of this gold standard method relies on precision thermal cycling, thus making it incompatible with on-chip analysis and difficult to adapt to many important diagnostic applications. Therefore, this limitation strongly justifies a quest for isothermal DNA amplification alternatives.[2,3] Rolling circle amplification (RCA) among all isothermal DNA amplification methods, such as loop-mediated isothermal amplification,[4] nucleic acid sequence-based amplification,[5] and signal mediated amplification of RNA technology,[6] is one of the simplest, most powerful, and versatile techniques. In contrast to PCR, which relies on linear, double-stranded DNA (dsDNA) templates, RCA utilizes a circular oligonucleotide as a template for a strand displacing DNA polymerase, such as Phi29. The Phi29 polymerase produces a long repeating product strand that serves as amplified copies of the circle sequence.[7,8] The RCA offers several unique features that give it an advantage over conventional PCR-based processes. RCA does not need costly temperature cyclers or any other specialized instrumentation. Simplicity, short assay time, high sensitivity, and selectivity make this technique ideal for the low-cost and point-of-care diagnostics. Moreover, besides simplicity, RCA is compatible with all sorts of platforms, which makes it suitable for sensitive monitoring of a wide selection of infectious diseases.[9,10]

RCA-based assays are mainly analysed by quantification of the reaction products utilizing fluorescent measurements,[11–13] nanoparticle labeling,[13–16], or enzyme linkage.[16,17] This, in turn, enables monitoring of the reaction in real-time, but introduces additional materials and sample processing steps. Thus, it complicates the procedure, increases its time, as well as the cost of the assay, and limits the sensitivity of the method. However, thanks to the isothermal nature of RCA processes, there have been a few attempts to combine RCA with microfluidic platforms[18,19] or sensing schemes based on surface

[1] *Warsaw University of Technology, Institute of Microelectronics and Optoelectronics, Koszykowa 75, 00-662, Warszawa, Poland*
[2] Gdansk University of Technology, Faculty of Electronics, Telecommunications and Informatics, Department of Metrology and Optoelectronics, Narutowicza 11/12, 80-233 Gdansk
[3] INRS Centre Armand-Frappier Santé Biotechnologie, 531 boulevards des Prairies Laval (QC) Canada
[4] National Institute of Telecommunications, Szachowa 1, 04-894, Warszawa, Poland
[5] Photonic Research Centre, University of Quebec in Outaouais, 101 rue Saint-Jean-Bosco, Gatineau (QC), Canada
‡ Monika Janik and Seyed Vahid Hamidi contributed equally as first authors in this article.

plasmon resonance (SPR),[14,20] electrochemistry,[21] and electrochemiluminescence.[22] Even though some of these sensing systems reached aM limits of detection for DNA, most of them require additional signal enhancement. To reach those detection limits, e.g., nanoparticles or additional enzymatic cleavage reactions have been utilized. To maximize the RCA potential in molecular diagnostics, we sought to reduce technical complications and simplify the sensing procedure. It was achieved by combining RCA with a reliable, highly sensitive, and compact sensor, embedded in an optical fiber. Despite the recent advance in fiber optic sensors along with their intrinsic benefits, such as immunity to electromagnetic interference, the possibility of multiplexing, the capacity for remote measurement, the high compatibility with telecom optoelectronic devices, the low power consumption, high resistance to harsh environmental conditions (including corrosive chemicals) and long-term reliability, to date, optical fiber sensors have not been utilized to monitor isothermal DNA amplification.

Designed for this experiment optical fiber sensor is 60 µm in diameter and about 62.5 µm deep microcavity. The microstructure is fabricated by a femtosecond laser ablation in a standard telecommunication fiber forming a microcavity in-line Mach Zehnder interferometer (µIMZI). Such a structure facilitates the analysis of liquid samples of picoliter volumes. The microstructure splits light guided in the fiber into two parts, where one continues to propagate inside the remaining part of the core (reference beam), while the other propagates through the cavity (sensing beam) (Figure 1a). Two beams interfere at the distant sidewall of the microcavity resulting in an interference pattern. The sensitivity of this system to changes in optical properties in the cavity, i.e., refractive index (RI), exceeds 20,000 nm/RIU[23]. It makes the sensor one of the most sensitive fiber-optic platforms to date.

In contrast to other fiber optic sensors, e.g., those based on fiber gratings[24] or SPR-based fiber optic sensors,[24] µIMZI's sensitivity and character of the obtained response strongly depend on whether the RI changes taking place close to the µIMZI bottom or away from it, i.e., in the microcavity's volume. The spectral location of the transmission minimum – the mth-order interference dip, m is an integer (λ_m) – in the interference pattern can be described by Equation (1), where d is the diameter of the microcavity, $\Delta n_{eff} = n_{co} - n_{cl}$ is the difference between the effective RI of the two interfering modes, namely n_{co}, and n_{cl} in the remaining part of the fiber core and micromachined circular cavity, respectively, and φ_0 represents the initial phase.

$$\lambda_m = \frac{2\pi d \Delta n_{eff}}{(2m+1)\pi - \varphi_0} \quad (1)$$

Assuming the spectral shift relies mainly on Δn_{eff}, the response of the µIMZI can be influenced by two different effects delivering opposite outcomes. First, an increase in RI of the liquid within the microcavity volume influences mainly n_{cl}, thus inducing a spectral shift towards shorter wavelengths (Figure 1b1 and 1c1). On the other hand, change in RI at the microcavity's bottom affects the propagation in the remaining part of the core (n_{co}) inducing a shift of the spectrum towards longer wavelengths (Figure 1c2). This increase may result from, e.g., chemical functionalization of the surface, deposition of small biological materials, such as a peptide or DNA aptamers, or thin-film deposition (Figure 1b2)[25].

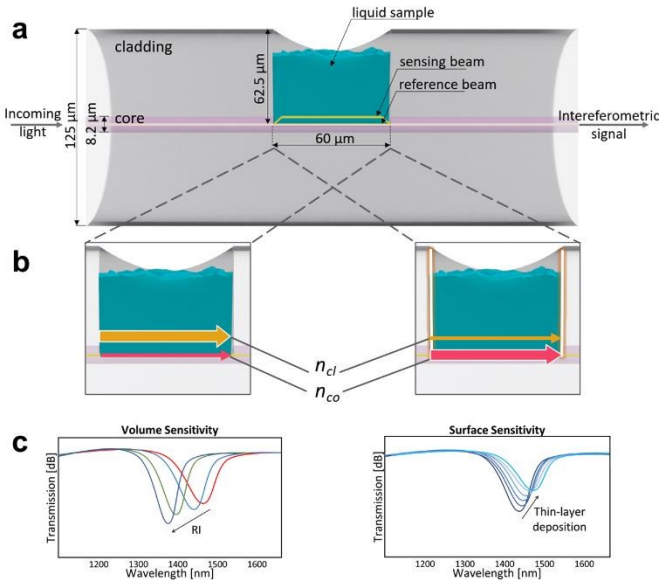

Figure. 1. a) A schematic illustration of the investigated µIMZI structure (cross-section view); b) Schematically shown two interfering modes – n_{co} in the remaining part of the fiber core, and n_{cl} in the micromachined cavity, influenced by the liquid inside the cavity and a thin layer, respectively. The drawings are not to scale; c) Exemplary transmission spectra of the µIMZI structure influences by RI changes and thin-layer thickness. Arrows indicate the shift of the minimum induced by each process.

In this proof-of-concept research, a pre-circularized DNA (circDNA) designed in our previous work[26] targeting the H5N1 influenza virus was employed as a sample target to develop an optical-fiber-based RCA monitoring technique. Combination of µIMZI and RCA enables users to monitor the detection via the amplification process in (1) real-time without labels or additional signal enhancers, (2) a pL volume (as a volume of the biological samples are often highly limited and intended for more than one test), and (3) with the highest possible selectivity and sensitivity detecting as little as hundreds of target copies.

Results and discussion

The µIMZI characterization

Each µIMZI utilized in this work was precisely micromachined following the optimized parameters described in Section 4.1. Figure 2a presents SEM visualization of one of the µIMZI. The whole surface of the structure is smooth, well-defined, the bottom is flat and precisely micromachined, and no additional damages are introduced to the cavity or the working area.

The microfabrication was followed by the RI sensitivity measurements of the µIMZIs. The measurements were performed on specially prepared hydrophobic test surfaces which allowed precise control of the amount of dosed liquid and filling of the microcavity. Figure 2b presents the transmission spectra of one of the chosen µIMZI samples where RI filling the cavity varied in the range from 1.3333 to 1.3496 RIU. Both the

transmitted power and the wavelength of the minima change with RI. The minimum shifts towards shorter wavelengths with RI what illustrates the volume sensing effect (Figure 1c1). In Figure 2c, the corresponding values of the spectral minima are plotted vs RI. The points corresponding to each of the samples are linearly approximated with the least square method, and the sensitivity in the chosen RI region is obtained. The fabricated interferometric structures reveal high linearity (R^2=0,997) of the RI sensitivity.

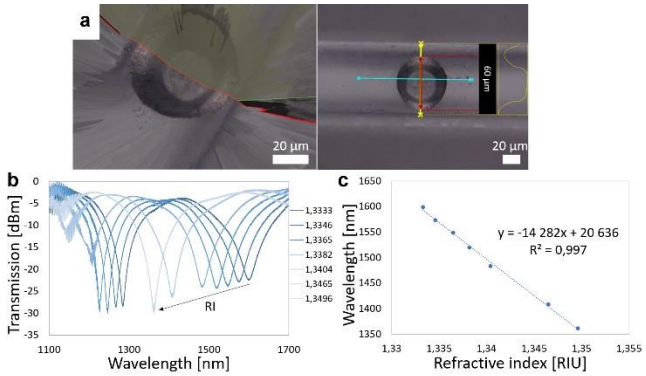

Figure 2. (a) A SEM pictures (top view) where the red arrow indicates the diameter of the microcavity, and yellow and blue arrows indicate the area subjected to scanning. RI sensitivity of the µIMZI where **(b)** shows transmission spectra of µIMZI filled with RI ranging from 1.3333 to 1.3496 RIU and **(c)** shows corresponding minimum wavelengths (marked by the black arrow in Figure 2b) plotted vs RI.

Chemical modification of the µIMZI's surface

To initiate the RCA reaction, the targeted DNA needs to hybridize with specific primers. This pair creates a binding site for DNA polymerase and enabling the DNA amplification. Therefore, to accommodate the RCA reaction inside the microcavity and be able to monitor the progress of the DNA amplification, both forward and reverse primers were immobilized on the µIMZI's surface. To ensure the covalent binding of the primers, the surface of the sensor was chemically modified (Section 4.2). The chemical modification was based on the two silanes, namely Triethoxysilylpropyl Succinic Anhydride (TESPSA) and (Azidopropyl)triethoxysilane (AzPTES) attached to the fiber's hydroxyl-coated surface by ethoxy groups. TESPSA has been used as a non-reactive linker to passivate the surface, while AzPTES with its azido group clicks with a DCBO group on DNA primer and thus forms a covalent bond between the DNA and the µIMZI surface. This surface treatment strategy based on click chemistry highly increased the efficiency of the subsequent immobilization of biological material. Furthermore, in contrast to typical NHS-ester chemistry relying on a terminal amine group on the primer,[27] it allowed us to avoid additional blocking of the surface.

During the following experimental steps, the µIMZI transmission spectra were monitored in range λ = 1100–1700 nm at a constant temperature of 24.3 degrees Celsius. Figure 3a presents the transmission spectra after each stage of the surface functionalization. The solid blue curve represents a readout before silanization; the solid red curve – after silanization with AzPTES and TESPSA, and the solid green curve represents the spectra after immobilization of the primers via click chemistry. The 30 min-long silanization process resulting in a shift of the minimum towards longer wavelengths by about 1.6 nm with a simultaneous increase in the transmission. Next, the primers' incubation step resulted in a 1.0 nm shift of the minimum also towards longer wavelengths what indicated the formation of the DNA-overlay on the surface of the microcavity. Figure 3b depicts an evolution of the wavelength corresponding to the transmission minimum at subsequent steps of surface functionalization along with primers' immobilization. Each measurement takes approx. 20 sec. It is worth mentioning that a sudden wavelength shift at the beginning of primers' immobilization (marked by a red arrow) is a result of an increase of RI of the sample. The further gradual shift of the spectrum towards shorter wavelengths is caused by the formation of the primers layer on the sensor's surface. This, in turn, changes the effective RI inside the microcavity and thus, the propagation conditions. At the end of the incubation, after extensive washing of the surface with PBS, the wavelength changes (designated as "Primers" in Figure 3b) revealing the influence of the formed DNA layer.

Done in parallel ccontact angle measurements allowed us to monitor the impact of silanization on the surface wettability (Figure 3c). Cleaning of the glass surface decreased the contact angle to the immeasurable value. Next, 30 min of chemical modification process increased it to 74.7° making the surface hydrophobic and indicating successful silanization of the surface.

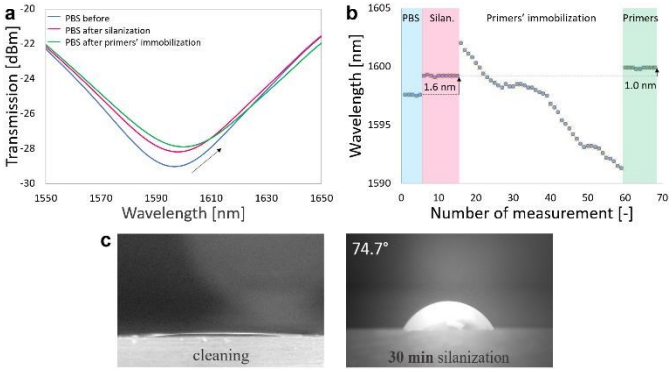

Figure 3. (a) Transmission spectra of the µIMZI at each stage of the surface functionalization, namely: in PBS before silanization, silanization with AzPTES and TESPSA, and immobilization of DNA primers via click chemistry. **(b)** Wavelength corresponding to the transmission minimum at subsequent steps of surface functionalization. For further analysis, only measurements performed in PBS were considered ("PBS", "Silan", "Primers"). **(c)** Photographic images of water droplet deposited on the glass surface after cleaning and after 30 min silanization processes.

RCA reaction mechanism

Functionalized µIMZI sensors were ready to proceed with the amplification reaction. The reaction started with the addition of an amplification mixture consisting of key elements. First, the circDNA – circular template/DNA target, the enzyme Phi29 DNA polymerase, and deoxynucleotide triphosphates (dNTPs) used to synthesize the new DNA strand. The components were diluted in a buffer solution which provides a suitable chemical environment for optimum activity and stability of the DNA polymerase. Finally, bovine serum albumin is added as an

adjuvant to stabilize the enzyme and preventing non-specific interactions.

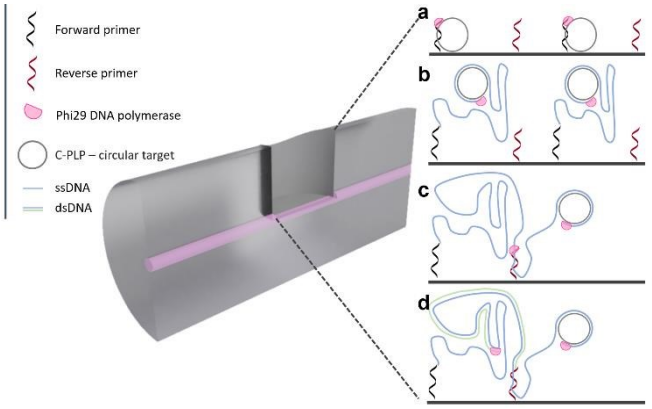

Figure 4. The schematic illustration of the RCA process inside the microcavity, where **(a)** shows hybridization of the circDNA to the forward primers followed by Phi29 DNA polymerase attachment, **(b)** DNA amplification, **(c)** complementary ssDNA product binding to the reverse primer, and **(d)** further DNA amplification with the use of the 3'OH group of the reverse primers.

The target circDNA described in our previous work[10,26] has an affinity to the forward primer immobilized on the µIMZI's surface. Thus, once specific hybridization between the target and forward primer on the microcavity's surface occurs (Figure 4a), Phi29 DNA polymerase starts DNA amplification from the 3´-hydroxyl group (OH) of the forward primer. When it reaches the starting point in the circular template it displaces the downstream strand and continues DNA polymerization (Figure 4b).[27,28] Therefore, the product of such amplification is a long tandemly repeated single-stranded DNA (ssDNA). Since the immobilized reverse primer is complementary to the long repeated single ssDNA (Figure 4c), it hybridizes with the produced ssDNA and brings it into the µIMZI's surface. These leads Phi29 DNA polymerase to also use 3´ OH groups of the hybridized reverse primer and perform further DNA amplification (Figure 4d). Because this newly synthesized strand is of the same sequence as the initial circDNA, the forward primer can once again hybridize to it to produce a new strand, and so on, hence a rapid exponential amplification. The final product of such isothermal DNA polymerization is double-stranded DNA which makes the process similar to conventional hyperbranched RCA (HRCA).[8,26]

The RCA real-time monitoring

The RCA process was monitored approx. every 20 sec. for 90 minutes. Each measurement corresponds to the 20 sec.-long intervals. Various circDNA concentrations starting from approximately 283 to 2 830 000 circDNA copies were applied. Within this experiment, we investigated the feasibility of performing a quantitative analysis of amplified DNA using the µIMZI sensor.

Figure 5a depicts the evolution of wavelength corresponding to the transmission minimum during the RCA monitoring and Figure 5b presents the exemplary spectral response (detection of 2 830 circDNA copies). As can be seen in Figure 5a, regardless of DNA concentration, the transmission minimum shifts towards shorter wavelengths with the progress of the RCA reaction, which is caused by the formation of the DNA in the microcavity.

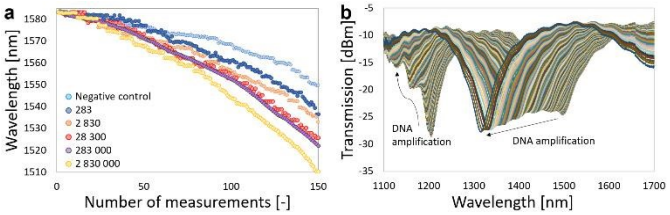

Figure 5. (a) The real-time µIMZI-based RCA monitoring diagram, where the concentration of the target varied from ca. 283 to 2 830 000 DNA copies. The negative curve (light blue line) resulted from a lack of phi29 polymerase. **(b)** Evolution of the transmission spectrum during the RCA process for the detection of 2 830 C-PLP copies. Arrows indicate the direction of the spectrum shift as it would be induced by increasing RI inside the microcavity.

The change of mass of the DNA sample affects the obtained spectra by significantly changing the density and viscosity of the analyzed sample. Incorporation of dNTPs into the DNA backbone produces protons and pyrophosphate as by-products,[9,10,29] which may also affect the RI of the analyte. Consequently, the effective RI within the sensing region increases affecting propagation conditions of the cladding mode, as is shown with the RI measurements in Figure 1b2 and c2.

Following the schema shown in Figure 4, one could expect that at the beginning of the amplification the spectrum will be affected mostly by changes on the µIMZI's surface. It means that the n_{co} in the remaining portion of the fiber core should be influenced by shifting the spectra towards longer wavelengths (as shown in Figure 1c2). However, following utilized chemical modification of the surface, therefore distribution of the primers on the sensor's surface it can be stated that initial changes of the DNA amplification are indistinguishable. By initial changes, we mean hybridization of the circDNA to the forward primers followed by Phi29 DNA polymerase attachment and the first minutes of the DNA amplification. The analysis of the RI shows that the amplification mixture and synthesized DNA on the µIMZI's surface are very close to the RI of the buffer. This further confirms that any observable shift of the minimum can be recorded once the amplified DNA starts changing the RI within the whole pL volume of the microcavity, thus affecting the cladding mode.

Initially, the process was monitored for 90 minutes to determine an appropriate timeframe for the identification of the RCA reaction. Initially, it was assumed that the length of the generated DNA strand would be proportional to the reaction time so the RI change should be proportional to the mass of products bounded to the sensor's surface. In spite of the fact that the shift does increase over time, very long amplification times do not appear to significantly improve the distinction between different starting concentrations of circDNA. Instead, it simply makes the experiment last longer, in contrast with a rapid assay which is more desirable for future development. The main reasons for that may be as follows. First, the same composition of the RCA reaction mixture (except for circDNA) limits the DNA concentration which can be synthesized during

View Article Online
DOI: 10.1039/D0LC01069C

the reaction. Thus, as can be seen in Fig. 5a, after a defined time, the placement of the transmission minimum approaches similar values, therefore decreasing R^2. Second, the µIMZI tracks the effective RI which is changing during the RCA reaction. However, primers are immobilized on the sensor's surface. As we reported in our previous work[25], the layer deposited on the sensor's surface increases its surface sensitivity at the expense of changes occurring further away from surface. Therefore, it is possible that overpacking the surface with dense DNA coverage may make the sensor less volume sensitive as further RI changes caused by DNA amplification are displaced away from the sensor's surface. In contrast, short reaction times limit spectral shifts of the minima and make detection difficult at low concentrations of the target.

To find the optimal reaction time, correlation coefficients between the initial concentrations of DNA targets, and the spectral shift of the minimum at varying amplification times were analyzed. Table 1 presents the correlation coefficients of the obtained response curves.

Table 1. Correlation coefficients of the experimental response curves obtained for the chosen time.

Time of DNA amplification [min]	Correlation coefficient R^2
10	0,5219
20	0,9338
30	0,9917
40	0,9782
50	0,9610
60	0,9251

It was found that from the correlation coefficient point of view (maximum R^2) the time between 30-40 min is the most appropriate and therefore was used for further analysis of the sensitivity of the method.

Negative control

The RCA reaction was also confirmed with two negative controls. The first one was conducted using the amplification mixture without an enzyme responsible for DNA amplification, and the second one was without the primers immobilized on the sensor's surface. Both cases result in a lack of DNA amplification. As both curves revealed the same trend, just the control without the enzyme was included in Figure 5a (light blue dots). The changes of the minimum wavelength for this sample likely resulted from the binding of the circDNA to the immobilized primers and slight evaporation of the reaction buffer. In comparison to the spectral change of the positive probes, the change of the RI was much smaller in this case, and the shift of the minimum was steady throughout the whole experiment. Moreover, to visualize the presence of DNA resulting from RCA reactions we have performed another test (Figure S1) that confirmed the surface functionalization, amplification, and thus detection method.

Sensitivity of the method

Figure 6a depicts the evolution of wavelength corresponding to the transmission minimum during the RCA monitoring over 30 to 40 minutes. The graph displays the recorded raw data (dots) and the fitted curves (solid lines). We used a gaussian fit with four terms for best shape projection and minimalization of data fluctuation.

To evaluate the sensitivity of this method, we investigated the relationship between the concentration of the target in the reaction mixture and the transmission shift of the minimum at 30 minutes using fitted data. The change of the resonance shift versus the copy number of the target (Figure 6b) revealed linear behavior within the whole investigated range starting from 283 to 2 830 000 copies of the DNA target (representing a concentration range from 9.4 aM to 94 pM). Following the obtained data, the experimental limit of the detection (LOD)

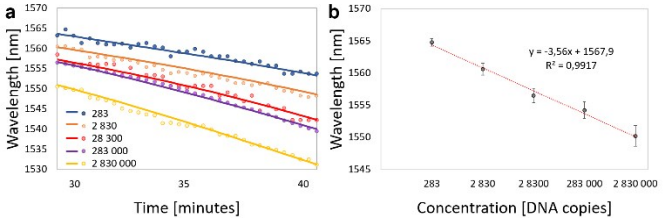

Figure 6. (a) Real-time µIMZI-based RCA monitoring plot for the period between 30 and 40 minutes, where raw data are present as dots, and the fitted curves as solid lines; **(b)** corresponding minimum wavelengths are plotted vs circDNA copy number showing the sensitivity of the performed experiment at 30 minutes. Error bars represent standard deviation (n = 5) for single experiment.

was set as 283 circDNA copies (9.4 aM), though the calculated LOD reached a remarkable value of 6 circDNA copies, which is equal to a circDNA concentration of 0.2 aM. To investigate the sensor resolution and repeatability especially for the lowest target concentrations, all the circDNA concentrations were run in triplicate under the same conditions, but with different microcavities. The calculated sensor-to-sensors relative standard deviation is equal to ~0.1% for all DNA concentrations suggesting both high resolution and reproducibility between the sensors.

The other recent optical RCA sensors have been based on SPR.[14,15,20] Although the detection limit of one of the probes presented by Huang et al.,[15] reached 20 aM and the reported system showed some disadvantages. First, the sensor required the measured signal enhancement using Au nanoparticles. Second, besides the nanoparticles, also enzymatic cleavage was utilized for the signal enhancement. In the other sensor developed by Xiang et al.,[14] the authors reported a similar SPR-based system incorporating RCA and Au nanoparticle, where they were able to reach a LOD of 5 pM with a synthetic DNA target. Shi et al.[30] reached LOD of 0.5 pM using synthetic nucleotides, however, the circDNA was attached to the sensor's surface indirectly through a nanoparticle and biotin-avidin interaction. The introduction of additional materials and sample

processing steps complicates the procedure, increases its time, as well as the cost of the assay. Furthermore, it can also influence the sensitivity of the method. Other reported RCA based sensors reached 0.28 fM using enzyme assisted electrochemical platforms[31] and 1.6 fM using an electrochemiluminescence sensor.[32] What is worth mentioning is real-time PCR, considered as a gold standard in detection methods. PCR offers a LOD around 384 DNA copies per mL (approximately 0.6 aM) with the H1N1 influenza virus.[33] This detection limit is comparable to the one reached in this work falling between the calculated LOD of 0.2 aM and the observed LOD of 9 aM in this study.

The biosensing system studied in this work offers distinct advantages over existing detection methods, such as PCR, ELISA, and cell culture, or a combination of those three. The use of RCA/HRCA combined with highly RI sensitive µIMZI makes the system ultra-sensitive. The DNA amplification additionally enhances the signal, making it possible to reach a low detection limit without a culturing step. Moreover, the presented approach is universally applicable, making the sensor suitable for the detection of any DNA target based on proper primer design.

Considering the size of the presented sensor, and the pL volume analysis, the assay is highly compatible with the point-of-care field application and may be multiplexed in the future targeting more than one DNA sequence. As the RCA is an isothermal reaction there is no need for additional equipment, e.g., thermoblocks. Furthermore, because of the high specificity and selectivity provided by the incorporation of multiple primers and necessary circular template, the system should work well with without any interference from other DNAs/RNAs present in the sample. Also, these results demonstrate that the analysis can provide rapid quantitative detection of DNA amplification. Indeed, several isothermal assays have been designed for point-of-care applications and many of these provide a qualitative measure, while µIMZI-RCA provides quantitative measurements over an extended time without compromising its outstanding sensitivity.

Conclusions

In summary, for the first time optical-fiber-based sensor – the microcavity in-line Mach-Zehnder interferometer – has been investigated for the real-time and label-free monitoring of isothermal DNA amplification. The reported method takes advantage of an outstanding sensitivity of the sensing platform, its capability for analysis of as low as picoliter volumes, and highly efficient chemical functionalization of the sensor's surface based on click chemistry reaction. The sensor achieved a linear range of detection between 283 – 2 830 000 DNA target copies, which corresponded to between 9.4 aM and 94 pM circDNA. Within just 30 min amplification duration as low as 238 copies (9.4 aM) of DNA target could be detected, while the calculated limit of the detection was equal to 6 DNA copies – 0.2 aM circDNA, thus, outperforming other sensors reported to date. Considering all the above, the presented sensor may find the practical application in point-of-care testing including early disease diagnosis.

View Article Online
DOI: 10.1039/D0LC01069C

Methods

All the DNA sequences and DNA target-related information were described in detail in our previous work.[9,10,26]

µIMZI fabrication and analysis

Sensing structures in the form of cylindrical cavities with a diameter of 60 µm were fabricated in standard Corning SMF-28e fibers following the one-step method described in detail in.[23,34,35] During the entire experiment, the µIMZI transmission was monitored in the spectral range of 1100-1700 nm with an NKT Photonics SuperK COMPACT supercontinuum white light source and a Yokogawa AQ6370C optical spectrum analyzer (the resolution of the optical spectrum analyzer was equal to 0.1 nm). To perform the reference RI sensitivity measurements a set of water/glycerin solutions with RI varied in the range of 1.3330–1.3496 RIU was used. The RI of the solutions was measured using a digital refractometer VEE GEE PDX-95.

µIMZI's surface functionalization

First, to remove contaminations and enhance the density of hydroxyl groups (Si-OH) on the surface the cavity was washed with 70% ethanol (Sigma-Aldrich) and milliQ water. Then the microcavity was filled with 1 M NaOH (Sigma-Aldrich) for 5 min. This step was followed by extensively washing of the surface consecutively with 70% ethanol, phosphate-buffered saline (PBS) (Sigma-Aldrich), and finally with miliQ water. Before surface silanization, 44.5 mg of 3-(Triethoxysilyl)propylsuccinic anhydride (TESPSA) (Oakwood Chemical, USA) and 6.08 mg of 3-(Azidopropyl)triethoxysilane (AzPTES) (Gelest, USA) were dissolved separately in 1 mL milliQ water. After mixing the two solutions (1:1, v/v), the microcavity was placed in the prepared mixture for 30 minutes. The effectiveness of the process was controlled by both the concentration of the precursor and exposure time. The sensor was then extensively washed consecutively in 70% ethanol, PBS, and milliQ water and dried at room temperature for 30 minutes. In the next step, the functionalization layer was cured at 105°C for 2 hours. Such a surface was ready for the click reaction. For the conjugation, the sensor was incubated in 10 µM DBCO-DNA primers (forward and reverse) solution for 1 hour. After this time, the surface of the microcavity was again extensively washed with 70% ethanol, PBS, and water to wash away non-attached primers. Finally, prepared microcavity was ready for monitoring of the RCA reactions. Figure 7 presents a schematic drawing of the surface functionalization.

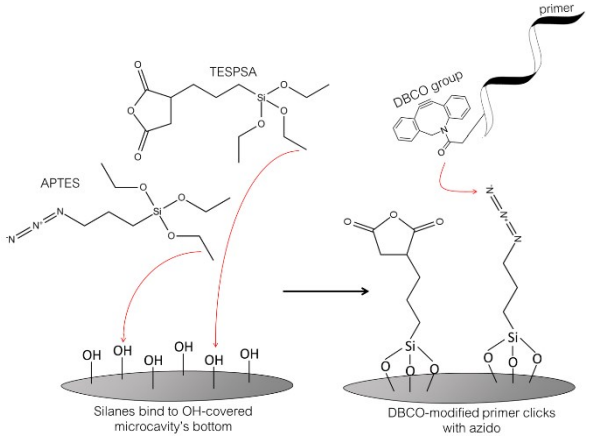

Figure. 7. Schematic drawing showing the surface functionalization of the µIMZI with copper-free click chemistry. First, TESPSA and AzPTES are attached to the -OH coated surface via ethoxy groups. TESPSA has been used as a non-reactive linker to passivate the surface, while AzPTES with its azido group clicks with a DCBO group on DNA primer and thus forms a covalent bond between the DNA and the µIMZI surface.

RCA reaction

The purified circDNAs were dissolved in milliQ water and then diluted to produce a serial dilution of circDNA so the RCA assay could be examined at several circDNA copy numbers**.** The RCA reaction was performed in a total volume of 90 µL consisting of 5 µL circDNA, 416 µM deoxyribonucleotide triphosphate (dNTP) (Thermo Fisher Scientific, USA), 68.4 µL milliQ water, 1X Phi29 DNA polymerase buffer (NEB), 30 µg bovine serum albumin – BSA (NEB), and 24 units of Phi29 DNA polymerase (NEB). Then 50 µL of the amplification mixture was incubated with the functionalized µIMZI for 90 minutes at room temperature. The temperature was controlled during the experiment with an accuracy of 0.06°C (HP 34970A Data Acquisition Unit). The experiment was monitored in real-time during the whole process.

Conflicts of interest

There are no conflicts to declare.

Acknowledgements

This work was supported by the National Science Center, Poland (NCN) (2018/29/B/ST7/02552), the Natural Sciences and Engineering Research Council of Canada [RGPIN-2019-06403], and the Canada Research Chairs Program; S.V. Hamidi received fellowships from Armand-Frappier foundation and Fonds québécois de la recherche sur la nature et les technologies (FRQNT). J.P. is a junior 2 FRQS research scholar.

References

1 K. B. Mullis, *Sci. Am.*, 1990, **262**, 56–65.
2 M. M. Ali, F. Li, Z. Zhang, K. Zhang, D. K. Kang, J. A. Ankrum, X. C. Le and W. Zhao, *Chem. Soc. Rev.*, 2014, **43**, 3324–3341.
3 Y. Zhao, F. Chen, Q. Li, L. Wang and C. Fan, *Chem. Rev.*, 2015, **115**, 12491–12545.
4 T. Notomi, Y. Mori, N. Tomita and H. Kanda, *J. Microbiol.*, 2015, **53**, 1–5.
5 X. Lu, X. Shi, G. Wu, T. Wu, R. Qin and Y. Wang, *Sci. Rep.*, 2017, **7**, 1–9.
6 P. J. Asiello and A. J. Baeumner, *Lab Chip*, 2011, **11**, 1420–1430.
7 V. V Demidov and H. Thorne, 2002, 542–548.
8 P. M. Lizardi, X. Huang, Z. Zhu, P. Bray-Ward, D. C. Thomas and D. C. Ward, *Nat. Genet.*, 1998, **19**, 225–232.
9 S. V. Hamidi and J. Perreault, *Talanta*, 2019, **201**, 419–425.
10 S. V. Hamidi and H. Ghourchian, *Biosens. Bioelectron.*, 2015, **72**, 121–126.
11 R. Ke, A. Zorzet, J. Göransson, G. Lindegren, B. Sharifi-Mood, S. Chinikar, M. Mardani, A. Mirazimi and M. Nilsson, *J. Clin. Microbiol.*, 2011, **49**, 4279–4285.
12 R. R. G. Soares, F. Neumann, C. R. F. Caneira, N. Madaboosi, S. Ciftci, I. Hernández-Neuta, I. F. Pinto, D. R. Santos, V. Chu, A. Russom, J. P. Conde and M. Nilsson, *Biosens. Bioelectron.*, 2019, **128**, 68–75.
13 K. W. Park, C. Y. Lee, B. S. Batule, K. S. Park and H. G. Park, *RSC Adv.*, 2018, **8**, 1958–1962.
14 Y. Xiang, K. Deng, H. Xia, C. Yao, Q. Chen, L. Zhang, Z. Liu and W. Fu, *Biosens. Bioelectron.*, 2013, **49**, 442–449.
15 Y. Xiang, X. Zhu, Q. Huang, J. Zheng and W. Fu, *Biosens. Bioelectron.*, 2015, **66**, 512–519.
16 H. Su, R. Yuan, Y. Chai, L. Mao and Y. Zhuo, *Biosens. Bioelectron.*, 2011, **26**, 4601–4604.
17 D. Zhu, Y. Yan, P. Lei, B. Shen, W. Cheng, H. Ju and S. Ding, *Anal. Chim. Acta*, 2014, **846**, 44–50.
18 Y. Jiang, S. Li, Z. Qiu, T. Le, S. Zou and X. Cao, *J. Food Saf.*, 2019, **39**, 1–9.
19 T. Yasui, K. Ogawa, N. Kaji, M. Nilsson, T. Ajiri, M. Tokeshi, Y. Horiike and Y. Baba, *Sci. Rep.*, 2016, **6**, 1–8.
20 Y. Y. Huang, H. Y. Hsu and C. J. C. Huang, *Biosens. Bioelectron.*, 2007, **22**, 980–985.
21 L. Zhou, L. J. Ou, X. Chu, G. L. Shen and R. Q. Yu, *Anal. Chem.*, 2007, **79**, 7492–7500.
22 Q. Su, D. Xing and X. Zhou, *Biosens. Bioelectron.*, 2010, **25**, 1615–1621.
23 M. Janik, A. K. Mysliwiec, M. Koba, A. Celebanska, W. J. Bock and M. Smietana, *IEEE Sens. J.*, , DOI:10.1109/JSEN.2017.2695544.
24 R. Correia, S. James, S. W. Lee, S. P. Morgan and S. Korposh, *J. Opt. (United Kingdom)*, , DOI:10.1088/2040-8986/aac68d.
25 M. Śmietana, M. Janik, M. Koba and W. J. Bock, *Opt. Express*, 2017, **25**, 26118–26123.
26 S. V. Hamidi, H. Ghourchian and G. Tavoosidana, *Analyst*, 2015, **140**, 1502–1509.
27 M. G. Mohsen and E. T. Kool, *Acc. Chem. Res.*, 2016, **49**, 2540–2550.
28 R. Johne, H. Müller, A. Rector, M. van Ranst and H. Stevens,

View Article Online
DOI: 10.1039/D0LC01069C

Trends Microbiol., 2009, **17**, 205–211.
29 N. A. Tanner, Y. Zhang and T. C. Evans, *Biotechniques*, 2015, **58**, 59–68.
30 D. Shi, J. Huang, Z. Chuai, D. Chen, X. Zhu, H. Wang, J. Peng, H. Wu, Q. Huang and W. Fu, *Biosens. Bioelectron.*, 2014, **62**, 280–287.
31 S. Wang, Y. Ji, H. Fu and H. Ju, 2019, 691–697.
32 Y. Lin, X. Huang, Y. Zhang, D. Chen, J. Wang and F. Luo, 2019, 827–833.
33 M. Panning, M. Eickmann, O. Landt, M. Monazahian, S. Ölschläger, S. Baumgarte, U. Reischl, J. J. Wenzel and H. H. Niller, 2009, 1–6.
34 M. Janik, S. Member, T. Eftimov, M. Koba, M. Smietana, W. J. Bock and L. Member, *J. Light. Technol.*, 2019, **37**, 4501–4506.
35 M. Janik, M. Koba, A. Celebańska, W. J. Bock and M. Śmietana, *Opt. Laser Technol.*, 2018, **103**, 260–266.

View Article Online
DOI: 10.1039/D0LC01069C

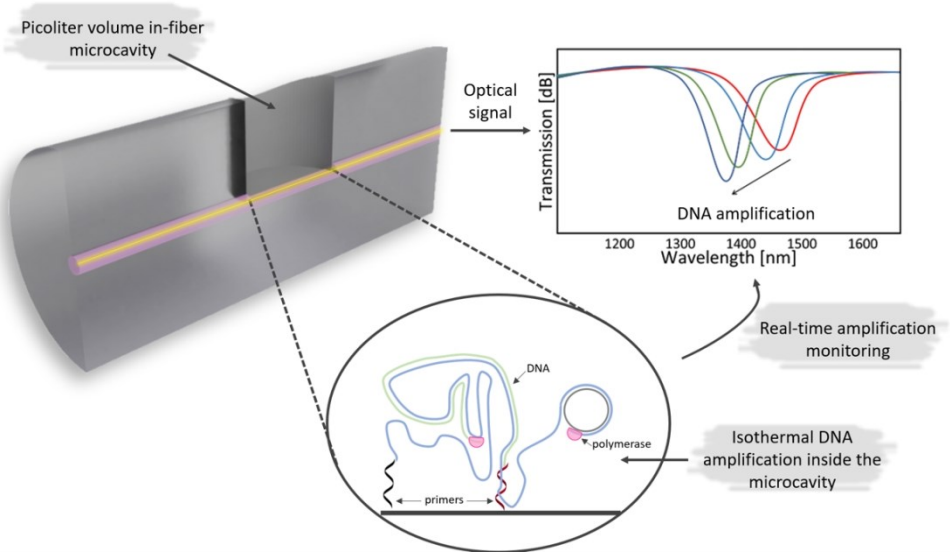

338x190mm (95 x 95 DPI)